The Intrinsic Temperature and Radiative–Convective Boundary Depth in the Atmospheres of Hot Jupiters

Daniel Thorngren[1,2] , Peter Gao[3,5] , and Jonathan J. Fortney[4]

[1] Department of Physics, University of California, Santa Cruz, CA, USA
[2] Institut de Recherche sur les Exoplanètes, Université de Montréal, Montréal, QC, Canada
[3] Department of Astronomy, University of California, Berkeley, CA, USA
[4] Department of Astronomy and Astrophysics, University of California, Santa Cruz, CA, USA

Abstract

In giant planet atmosphere modeling, the intrinsic temperature T_{int} and radiative–convective boundary (RCB) are important lower boundary conditions. Often in one-dimensional radiative–convective models and in three-dimensional general circulation models it is assumed that T_{int} is similar to that of Jupiter itself, around 100 K, which yields an RCB around 1 kbar for hot Jupiters. In this work, we show that the inflated radii, and hence high specific entropy interiors (8–11 k_b/baryon), of hot Jupiters suggest much higher T_{int}. Assuming the effect is primarily due to current heating (rather than delayed cooling), we derive an equilibrium relation between T_{eq} and T_{int}, showing that the latter can take values as high as 700 K. In response, the RCB moves upward in the atmosphere. Using one-dimensional radiative–convective atmosphere models, we find RCBs of only a few bars, rather than the kilobar typically supposed. This much shallower RCB has important implications for the atmospheric structure, vertical and horizontal circulation, interpretation of atmospheric spectra, and the effect of deep cold traps on cloud formation.

Unified Astronomy Thesaurus concepts: Exoplanet atmospheres (487); Extrasolar gas giants (509); Exoplanet structure (495); Exoplanet evolution (491)

1. Introduction

Soon after the discovery of strongly irradiated giant planets (Mayor & Queloz 1995), it was realized that they would have strikingly different atmospheres from the giant planets in our own solar system (Guillot et al. 1996; Seager & Sasselov 1998; Marley et al. 1999). For Jupiter at optical wavelengths, one can see down to the ammonia cloud tops (∼0.6 bars), which are within the convective region of the planet that extends into its vast deep interior. For hot Jupiters (with $T_{eq} > 1000$ K; see Miller & Fortney 2011), it was appreciated that their atmospheres could remain radiative to a considerably greater depth due to incident fluxes that are often thousands of times that of Earth's insolation, which force the upper atmosphere to a much higher temperature (typically 1000–2500 K) than for an isolated object (Guillot & Showman 2002; Showman & Guillot 2002; Sudarsky et al. 2003). This leads to a significant departure of the atmospheric temperature structure from an adiabat, and has major consequences for atmospheric circulation (Showman & Guillot 2002; Showman et al. 2008; Rauscher & Menou 2013; Heng & Showman 2015). As such, there has long been significant interest in understanding what controls the pressure level of the hot Jupiter radiative–convective boundary (RCB).

Radiative–convective atmosphere models for hot Jupiters found that, for Jupiter-like intrinsic fluxes (parameterized by T_{int}, of 100 K) but incident stellar fluxes 10^4 times larger, one typically found RCB pressures near 1 kbar (e.g., Guillot & Showman 2002; Sudarsky et al. 2003; Fortney et al. 2005). While it was understood early on that the RCB depth strongly depends on the value of T_{int} (e.g., Sudarsky et al. 2003, their Figure 16), cooling models suggested that T_{int} values would fall with time to Jupiter-like values (Guillot & Showman 2002;

Burrows et al. 2004; Fortney et al. 2007), and the ∼1 kbar RCB became ensconced as a "typical" value for these objects. Such atmospheres are very different from those found in the solar system, so considerable modeling effort has gone into studying their possible vertical and horizontal circulation patterns, and to what degree cold traps at depth may affect what molecules and cloud species can be seen in the visible layers (Hubeny et al. 2003; Fortney et al. 2008; Powell et al. 2018).

However, the larger than expected radii of hot Jupiters suggest interiors that are much hotter and more luminous than our own Jupiter (e.g., Guillot & Showman 2002). This is because even a pure H/He object at Jupiter's internal temperatures cannot match the observed radii of hot Jupiters (Fortney et al. 2007; Miller & Fortney 2011). This implies higher interior fluxes and shallower—sometimes much shallower—RCB boundaries than the canonical 1 kbar. Such atmospheres have occasionally appeared in other works (e.g., Guillot 2010; Sing et al. 2016; Komacek & Youdin 2017; Tremblin et al. 2017), but were not studied extensively. In this work, we will quantify interior fluxes and the RCB depth as a function of planetary T_{eq} to better inform the thermal structure of 1D and 3D atmosphere models.

2. Modeling

We will parameterize the rate at which heat escapes from a planet's deep interior using the intrinsic temperature T_{int}. Its value is primarily driven by the entropy of the underlying adiabat. Thus, high T_{int} is typical of young exoplanets and inflated hot Jupiters. If the mechanism inflating hot Jupiters involves the deposition of heat into the interior, then they will eventually reach a thermal equilibrium where $E_{in} = E_{out}$. The hotter the planet, the faster this equilibrium will be reached, in as little as tens of megayears (Thorngren & Fortney 2018). Once equilibrium is reached, the intrinsic temperature is a
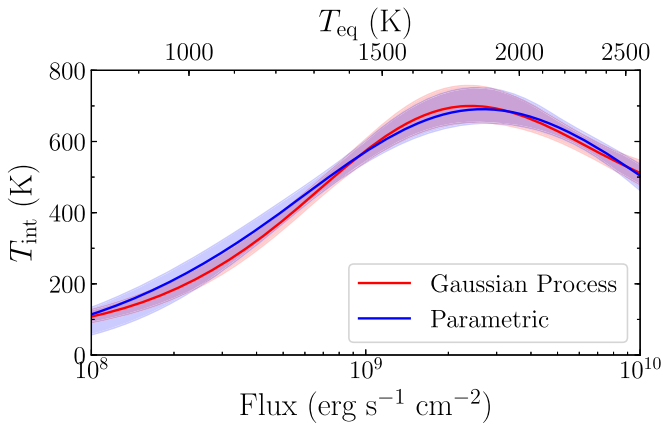
Figure 1. Intrinsic temperatures of hot Jupiters in equilibrium as a function of incident flux (bottom) or equilibrium temperature (top). These were derived from the two favored heating models (Gaussian process and Gaussian parametric) of Thorngren & Fortney (2019), using Equation (2), with corresponding uncertainties. The two models yield nearly identical results. Importantly, the intrinsic temperatures must be quite high—up to 700K—to match the hot interiors required to explain the radii of hot Jupiters.

function of the equilibrium temperature:

$$4\pi R^2 \sigma T_{int}^4 = \pi R^2 F \; \epsilon(F), \qquad (1)$$

$$T_{int} = \left(\frac{F \; \epsilon(F)}{4\sigma} \right)^{\frac{1}{4}} = \epsilon(F)^{\frac{1}{4}} T_{eq}, \qquad (2)$$

$$\approx 1.24 \; T_{eq} \exp\left(-\frac{(\log(F) - 0.14)^2}{2.96} \right). \qquad (3)$$

Here, F is the incident flux on the planet (so $F = 4\sigma T_{eq}^4$), σ is the Stefan–Boltzmann constant, and ϵ is the fraction of the flux that heats the interior. This varies with flux, and was inferred by matching model planets with the observed hot Jupiter population in Thorngren & Fortney (2018). The resulting intrinsic temperatures are shown in Figure 1, and the associated entropies (which depend on mass and composition) are shown in Figure 2.

The high intrinsic temperatures this relation produces are important due to the effect they have on the atmosphere. In particular, the radiative–convective boundary moves to lower pressures for higher T_{int}. In contrast, larger T_{eq} tends to push the RCB to higher pressures. As these temperatures are related, it is not immediately obvious where the RCB ends up for planets at high equilibrium temperatures. To evaluate the RCB depth, we generate model atmospheres using a well-established thermal structure model for exoplanets and brown dwarfs (e.g., McKay et al. 1989; Marley et al. 1996, 1999; Fortney et al. 2005, 2008; Saumon & Marley 2008; Morley et al. 2012). The model computes temperature–pressure (TP) and composition profiles assuming radiative–convective–thermochemical equilibrium, taking into account the depletion of molecular species due to condensation.

Model atmospheres are generated for a grid of cloud-free giant exoplanets with 1 bar gravities of 4, 10, 25, and 75 m s^{-2} and a range of T_{eq} from ∼700 to ∼2800 K (Figure 3). These were chosen to bracket the gravity and T_{eq} of nearly all observed hot Jupiters. Values of T_{eq} were computed assuming full heat redistribution, meaning that incoming stellar radiation is reradiated from the entire planetary surface. Functionally, we positioned the model planets at various semimajor axes around a
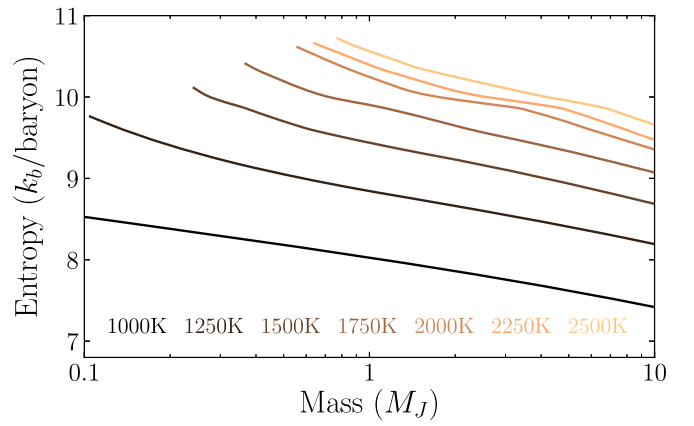

Figure 2. Equilibrium entropy of hot Jupiters as a function of their mass for various equilibrium temperatures. Each line has models of the same intrinsic and equilibrium temperature, but variations in the resulting surface gravity lead to different internal entropies. In particular, heat escapes more efficiently through the compact atmospheres of massive objects for a given T_{int}. The composition was assumed to be typical (from Thorngren et al. 2016), using the SCvH (Saumon et al. 1995) and ANEOS 50-50 rock-ice (Thompson 1990) equations of state; different compositions will shift the entropy somewhat.
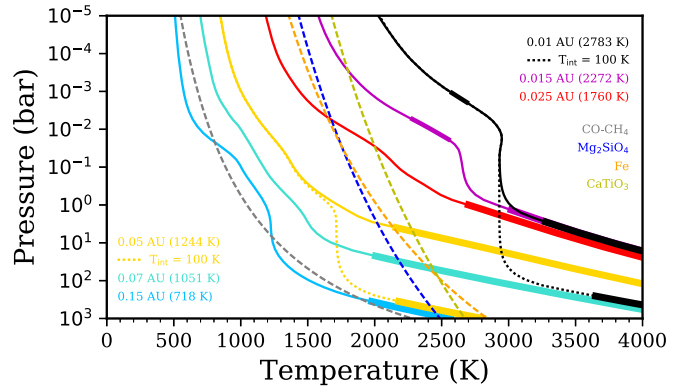

Figure 3. Selected pressure–temperature profiles of our 10× solar atmospheric metallicity models for various semimajor axes around a Sun-like star and the resulting T_{eq} (in brackets), from which we derive the intrinsic temperature. The 1 bar gravity is set to 10 m s^{-2}. The thick lines indicate convective regions, whereas thin lines correspond to radiative regions. Alternative pressure–temperature profiles for a T_{int} = 100 K model for the 0.05 au and 0.01 au cases are plotted as dotted curves. The condensation curves for Mg_2SiO_4, $CaTiO_3$, and iron are shown as dashed curves; T_{int} can be seen to strongly affect their condensation pressures. The CO–CH_4 coexistence curve (Visscher 2012) is also shown; in general, hot Jupiters should be well on the CO side. In the hottest cases, a second convective region forms; however, we will use the term RCB to refer exclusively to the outer edge of the interior adiabatic envelope. This boundary is visible in the plot for the profiles given, and moves to lower pressures at higher equilibrium temperatures.

Sun-like star. Two grids were computed, one assuming solar atmospheric metallicity and one assuming 10× solar atmospheric metallicity (similar to Saturn), with any additional heavy elements sequestered in a core, such that the bulk metallicities matched the median of the observed mass–metallicity relationship given by Thorngren et al. (2016). The RCB depth for each model planet is then defined, when traveling from the deep interior into the atmosphere, as the first pressure level where the local lapse rate transitions from adiabatic to subadiabatic.

We calculate the masses, radii, and adiabat entropies (Figure 2) of our model planets (from the gravity and T_{eq}) using the planetary interior model of Thorngren & Fortney (2018), which solves the equations of hydrostatic equilibrium, mass and energy
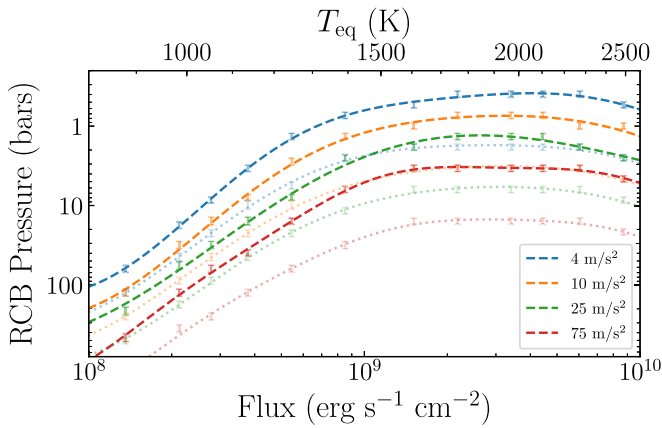
Figure 4. RCB pressure as a function of incident flux (or T_{eq}), shown for different surface gravities (colors; see the legend) and 1× (pale dotted) and 10× (dashed) solar metallicity atmospheres. Due to binning effects, there are small uncertainties around the modeled points, so we drew smooth lines through the data using Gaussian process interpolation with a squared exponential kernel whose parameters were optimized via the maximum likelihood.

conservation, and an appropriately chosen equation of state (EOS). We use the SCvH (Saumon et al. 1995) EOS for a solar ratio mixture of hydrogen and helium, and the ANEOS 50-50 rock-ice EOS (Thompson 1990) for the metals.

3. Results and Discussion

Our results for the location of the RCB are shown in Figure 4. The RCB moves to *lower pressures at higher equilibrium temperatures*, roughly in line with how T_{int} varies with T_{eq}. At the inflation cutoff of around 1000 K (Miller & Fortney 2011), the RCB is found at around 100 bars. At the extremum around $T_{eq} = 1800$ K, it is found at roughly 1 bar. Higher gravity moves the RCB to higher pressures, and higher metallicity moves it to lower pressures. At equilibrium, no hot Jupiter with gravity <25 m s^{-2} and solar or supersolar atmospheric metallicity should have an RCB as deep as 1 kbar.

3.1. Relation to the Heating Mechanism

These results have important implications for understanding the anomalous heating of hot Jupiters. Heating deposited below the RCB is much more effective for inflating planets than heat deposited above (Batygin & Stevenson 2010; Komacek & Youdin 2017). This is particularly important for ohmic dissipation. For the lower RCB pressures that we predict, models like ohmic dissipation will be more efficient than previously considered. Since giant planets are born quite hot, they will have RCBs at low pressures at young ages that could be maintained there by this heating. However, this would not necessarily allow for reinflation of a planet whose interior has already cooled (see Lopez & Fortney 2016), as the RCB might already be at tens of bars or deeper when the heating started. We refer the reader to Komacek & Youdin (2017) for a more detailed and broader discussion of these heating deposition depth effects.

It is also worthwhile to consider the effect that our assumptions about the hot Jupiter heating have on the model. In Thorngren & Fortney (2018), it was assumed that the heating was proportional to and a function of the incident flux, based on the results of Weiss et al. (2013). There may be additional factors that affect the heating, such as planet and stellar mass, but since $\epsilon(F)$ seems to predict planetary radii quite well, these

likely add at most modest uncertainty to our estimates of T_{int}. An additional consideration is whether the anomalous radii are caused entirely by heating, or whether there is a delayed cooling effect as well; for example, ohmic dissipation (Batygin et al. 2011) may be a combination of these (Wu & Lithwick 2013; Ginzburg & Sari 2016). Delayed cooling effects would alter the apparent T_{int} for a given internal adiabat entropy, and delay arrival at thermal equilibrium. However, many anomalous heating models do not rely on delayed cooling (e.g., Arras & Socrates 2009; Youdin & Mitchell 2010; Tremblin et al. 2017), and signs of possible reinflation (Grunblatt et al. 2016, 2017; Hartman et al. 2016) seem to favor these. If reinflation is conclusively shown to occur, then anomalous heating must be the dominant cause of radius inflation (Lopez & Fortney 2016), and our T_{int} estimates will be particularly good. Finally, the usual uncertainties in the EOS (see, e.g., Militzer & Hubbard 2013; Chabrier et al. 2019) and planet interior structure (Baraffe et al. 2008; Leconte & Chabrier 2012) discussed in Thorngren et al. (2016) also apply to this work.

3.2. Effect on Atmospheric Models

These results have important implications for global circulation models (GCMs) of hot Jupiters. It has long been a convention in this field to use intrinsic temperatures similar to Jupiter's (e.g., Showman et al. 2015; Amundsen et al. 2016; Komacek et al. 2017; Lothringer et al. 2018; Flowers et al. 2019, and many others), around 100 K (Li et al. 2012). Our work shows that more realistic values for T_{int} should depend strongly on the incident flux and will typically be several hundreds of Kelvin, as shown in Figure 1. This difference is important for vertical mixing and circumplanetary circulation, as it shifts the RCB to considerably lower pressures. It was recently demonstrated in the hot Jupiter context that changing the lower boundary conditions can yield significantly different atmospheric flows in these simulations (see Carone et al. 2019).

The higher implied intrinsic fluxes could also impact interpretations of the observed flux from hot Jupiters. For phase curves, night-side fluxes will be a mix of intrinsic fluxes, which in many cases can no longer be thought of as negligible, in addition to energy transported from the day side. Even on the day side, in near-infrared opacity windows that probe deeply, one might be able to observe this intrinsic flux as a small perturbation on the day-side emission spectrum (e.g., Fortney et al. 2017)

The value of T_{int} is also important for the location and abundance of condensates in hot Jupiter atmospheres. Figure 3 compares the condensation curves of several species, including forsterite, iron, and perovskite, to our model TP profiles; the intersection between the condensation curve and the TP profile delineates the cloud bases. Previous works that considered low T_{int} atmospheres have hypothesized the existence of deep "cold traps" for hot Jupiter clouds, where a cloud base at high pressures (>100 bars) removes condensates and condensate vapor from the visible layers of the atmosphere (e.g., Spiegel et al. 2009; Parmentier et al. 2016). However, higher T_{int} values increase deep atmospheric temperatures, such that the cloud base is much shallower in the atmosphere. For example, whether a planet with $T_{eq} = 1244$ K has a $T_{int} = 100$ K or our nominal value changes the forsterite cloud base pressure by ∼2 dex (Figure 3). This can have important observable consequences, particularly in emission, where the lack of deep cold

traps could result in cloudier day-side atmospheres (Powell et al. 2018).

A lack of deep cold traps can also prevent atomic metals in the visible atmosphere from being lost to deep clouds. While this Letter was under review, Sing et al. (2019) published the detection of singly ionized Mg and Fe in the transmission spectrum of WASP-121b. The fact that these metals are not cold trapped out of the planet's atmosphere at depth in forsterite and/or iron clouds strongly suggests that the shallow RCB suggested here is correct, at least for this planet (as shown in their Figure 13).

A related effect is the role of the RCB depth in affecting nonequilibrium chemical abundances. For instance, it is now well established that CO–CH_4 abundances are typically out of equilibrium in cool gas giants and brown dwarfs due to the mixing times being faster than the timescale for CO to convert to CH_4 (Cooper & Showman 2006; Moses et al. 2011; Zahnle & Marley 2014; Drummond et al. 2018). For the cooler planets modeled in Figure 3, if the quench pressure is ∼10–1000 bars (for instance), then the disequilibrium chemical abundances will differ when the RCB is moved (see also Drummond et al. 2018), as the local TP profile in the deep atmosphere will move in reference to the local CO–CH_4 equal abundance curve. This effect could be seen in the potential detectability of CH_4 in only the very coldest planets modeled here, where the upper atmosphere and deep atmospheres are both relatively cool.

3.3. Observational Tests and Future Work

We suggest several approaches to further verify our findings observationally. The previously supposed T_{int} of 100K could be ruled out if clouds are detected when they would otherwise be cold trapped, particularly for planets with $T_{eq} \sim 1100$–$1600\,K$ (see, e.g., Lines et al. 2018, or Figure 3). Similarly, low-pressure RCBs for hotter objects would lead to the presence of atomic metals or other gaseous species in the upper atmosphere that would otherwise be lost to deep cloud formation (Sing et al. 2019). In addition, CO-dominated (rather than CH_4-dominated) atmospheres across a wide T_{eq} range (at least for solar-like C/O ratios), including nearly all models shown in Figure 3, would suggest lower-pressure RCBs. Transmission and emission spectroscopy are well suited to these characterization tasks and the higher precision that will be attained with the *James Webb Space Telescope* will be important in this area. More directly, as suggested by Fortney et al. (2017), high intrinsic fluxes may be measured directly by higher fluxes in the near-IR, particularly in windows in water opacity. Finally, recent detections of strong magnetic fields suggest that high intrinsic temperatures are the reality (Yadav & Thorngren 2017; Cauley et al. 2019), since intrinsic temperature is tied to magnetic field strength (Christensen et al. 2009). This work now needs to be tied back into revised estimates for the ohmic dissipation that occurs in these atmospheres.

Future work should focus on the effects that these altered boundary conditions have on the cloud structure, chemical abundances, spectra, and day–night contrasts of hot Jupiters. As we learn more about hot Jupiter interiors through theoretical developments, population studies (especially from new *TESS* discoveries) and potentially reinflated giants (Grunblatt et al. 2017), we can better characterize these important atmospheric boundary conditions.

ORCID iDs

Daniel Thorngren ⓘ https://orcid.org/0000-0002-5113-8558
Peter Gao ⓘ https://orcid.org/0000-0002-8518-9601
Jonathan J. Fortney ⓘ https://orcid.org/0000-0002-9843-4354

References

Amundsen, D. S., Mayne, N. J., Baraffe, I., et al. 2016, A&A, 595, A36
Arras, P., & Socrates, A. 2009, arXiv:0901.0735
Baraffe, I., Chabrier, G., & Barman, T. 2008, A&A, 482, 315
Batygin, K., & Stevenson, D. J. 2010, ApJL, 714, L238
Batygin, K., Stevenson, D. J., & Bodenheimer, P. H. 2011, ApJ, 738, 1
Burrows, A., Hubeny, I., Hubbard, W. B., Sudarsky, D., & Fortney, J. J. 2004, ApJL, 610, L53
Carone, L., Baeyens, R., Mollière, P., et al. 2019, arXiv:1904.13334
Cauley, P. W., Shkolnik, E. L., Llama, J., & Lanza, A. F. 2019, NatAs, 1, 408
Chabrier, G., Mazevet, S., & Soubiran, F. 2019, ApJ, 872, 51
Christensen, U. R., Holzwarth, V., & Reiners, A. 2009, Natur, 457, 167
Cooper, C. S., & Showman, A. P. 2006, ApJ, 649, 1048
Drummond, B., Mayne, N. J., Manners, J., et al. 2018, ApJL, 855, L31
Flowers, E., Brogi, M., Rauscher, E., Kempton, E. M.-R., & Chiavassa, A. 2019, AJ, 157, 209
Fortney, J. J., Marley, M. S., & Barnes, J. W. 2007, ApJ, 659, 1661
Fortney, J. J., Marley, M. S., Lodders, K., Saumon, D., & Freedman, R. 2005, ApJL, 627, L69
Fortney, J. J., Marley, M. S., Saumon, D., & Lodders, K. 2008, ApJ, 683, 1104
Fortney, J. J., Thorngren, D., Line, M. R., & Morley, C. 2017, AAS/DPS Meeting, 49, 408.04
Ginzburg, S., & Sari, R. 2016, ApJ, 819, 116
Grunblatt, S. K., Huber, D., Gaidos, E., et al. 2017, AJ, 154, 254
Grunblatt, S. K., Huber, D., Gaidos, E. J., et al. 2016, AJ, 152, 185
Guillot, T. 2010, A&A, 520, A27
Guillot, T., Burrows, A., Hubbard, W. B., Lunine, J. I., & Saumon, D. 1996, ApJL, 459, L35
Guillot, T., & Showman, A. P. 2002, A&A, 385, 156
Hartman, J. D., Bakos, G. Á., Bhatti, W., et al. 2016, AJ, 152, 182
Heng, K., & Showman, A. P. 2015, AREPS, 43, 509
Hubeny, I., Burrows, A., & Sudarsky, D. 2003, ApJ, 594, 1011
Komacek, T. D., Showman, A. P., & Tan, X. 2017, ApJ, 835, 198
Komacek, T. D., & Youdin, A. N. 2017, ApJ, 844, 94
Leconte, J., & Chabrier, G. 2012, A&A, 540, A20
Li, L., Baines, K. H., Smith, M. A., et al. 2012, JGRE, 117, E11002
Lines, S., Manners, J., Mayne, N. J., et al. 2018, MNRAS, 481, 194
Lopez, E. D., & Fortney, J. J. 2016, ApJ, 818, 4
Lothringer, J. D., Barman, T., & Koskinen, T. 2018, ApJ, 866, 27
Marley, M. S., Gelino, C., Stephens, D., Lunine, J. I., & Freedman, R. 1999, ApJ, 513, 879
Marley, M. S., Saumon, D., Guillot, T., et al. 1996, Sci, 272, 1919
Mayor, M., & Queloz, D. 1995, Natur, 378, 355
McKay, C. P., Pollack, J. B., & Courtin, R. 1989, Icar, 80, 23
Militzer, B., & Hubbard, W. B. 2013, ApJ, 774, 148
Miller, N., & Fortney, J. J. 2011, ApJL, 736, L29
Morley, C. V., Fortney, J. J., Marley, M. S., et al. 2012, ApJ, 756, 172
Moses, J. I., Visscher, C., Fortney, J. J., et al. 2011, ApJ, 737, 15
Parmentier, V., Fortney, J. J., Showman, A. P., Morley, C., & Marley, M. S. 2016, ApJ, 828, 22
Powell, D., Zhang, X., Gao, P., & Parmentier, V. 2018, ApJ, 860, 18
Rauscher, E., & Menou, K. 2013, ApJ, 764, 103
Saumon, D., Chabrier, G., & van Horn, H. M. 1995, ApJS, 99, 713
Saumon, D., & Marley, M. S. 2008, ApJ, 689, 1327
Seager, S., & Sasselov, D. D. 1998, ApJL, 502, L157
Showman, A. P., & Guillot, T. 2002, A&A, 385, 166
Showman, A. P., Lewis, N. K., & Fortney, J. J. 2015, ApJ, 801, 95
Showman, A. P., Menou, K., & Cho, J. Y.-K. 2008, in ASP Conf. Ser. 398, Extreme Solar Systems, ed. D. Fischer (San Francisco, CA: ASP), 419

Sing, D. K., Fortney, J. J., Nikolov, N., et al. 2016, Natur, 529, 59
Sing, D. K., Lavvas, P., Ballester, G. E., et al. 2019, AJ, 158, 91
Spiegel, D. S., Silverio, K., & Burrows, A. 2009, ApJ, 699, 1487
Sudarsky, D., Burrows, A., & Hubeny, I. 2003, ApJ, 588, 1121
Thompson, S. L. 1990, ANEOS Analytic Equations of State for Shock Physics Codes Input Manual, Tech. Rep. SAND-89-2951, 6939284, Sandia National Laboratory, doi:10.2172/6939284
Thorngren, D., & Fortney, J. J. 2019, ApJL, 874, L31
Thorngren, D. P., & Fortney, J. J. 2018, AJ, 155, 214

Thorngren, D. P., Fortney, J. J., Murray-Clay, R. A., & Lopez, E. D. 2016, ApJ, 831, 64
Tremblin, P., Chabrier, G., Mayne, N. J., et al. 2017, ApJ, 841, 30
Visscher, C. 2012, ApJ, 757, 5
Weiss, L. M., Marcy, G. W., Rowe, J. F., et al. 2013, ApJ, 768, 14
Wu, Y., & Lithwick, Y. 2013, ApJ, 763, 13
Yadav, R. K., & Thorngren, D. P. 2017, ApJL, 849, L12
Youdin, A. N., & Mitchell, J. L. 2010, ApJ, 721, 1113
Zahnle, K. J., & Marley, M. S. 2014, ApJ, 797, 41

Erratum: "The Intrinsic Temperature and Radiative–Convective Boundary Depth in the Atmospheres of Hot Jupiters" (ApJL, 2018, 884, L6)

Daniel Thorngren[1,2], Peter Gao[3], and Jonathan J. Fortney[4]
[1] Department of Physics, University of California, Santa Cruz, USA
[2] Institut de Recherche sur les Exoplanètes, Université de Montréal, Canada
[3] 51 Pegasi b Fellow, Department of Astronomy, University of California, Berkeley, USA
[4] Department of Astronomy and Astrophysics, University of California, Santa Cruz, USA
Received 2020 January 15; published 2020 February 4

In the original published article, the constants in Equation (3) were incorrectly calculated. This did not affect other results in the paper because we were implicitly using the form in Equation (2); the error was only introduced when simplifying the equation for publication. As such, the other scientific results of the paper are unchanged. The corrected equations read:

$$4\pi R^2 \sigma T_{int}^4 = \pi R^2 F \ \epsilon(F) \tag{1}$$

$$T_{int} = \left(\frac{F \ \epsilon(F)}{4\sigma} \right)^{\frac{1}{4}} = \epsilon(F)^{\frac{1}{4}} T_{eq} \tag{2}$$

$$\approx 0.39 \ T_{eq} \exp \left(-\frac{(\log(F) - .14)^2}{1.095} \right). \tag{3}$$

Of these, only Equation (3) is different—the others are shown for context. Previously, the overall coefficient (now 0.39) was 1.24, and the power's denominator (now 1.095) was 2.96. Using the previous, incorrect values yields implausibly hot intrinsic temperatures of nearly 2000 K in the worst cases.

ORCID iDs

Daniel Thorngren ● https://orcid.org/0000-0002-5113-8558
Peter Gao ● https://orcid.org/0000-0002-8518-9601
Jonathan J. Fortney ● https://orcid.org/0000-0002-9843-4354